Unexpected Competition between Ferroelectricity and Rashba Effects in Epitaxially Strained $SrTiO_3$

Julien Varignon
CRISMAT, ENSICAEN, Normandie Université, UNICAEN, CNRS, 14000 Caen, France

(Received 1 May 2023; accepted 30 January 2024; published 7 March 2024)

The Rashba parameter α_R is usually assumed to scale linearly with the amplitude of polar displacements by construction of the spin-orbit interaction. On the basis of *first-principles* simulations, ferroelectric phases of $SrTiO_3$ reached under epitaxial compressive strain are characterized by (i) large Rashba effects at the bottom of the conduction band near the paraelectric-ferroelectric boundary and (ii) an unexpected suppression of the phenomena when the amplitude of polar displacements increases. This peculiar behavior is ascribed to the inverse dependence of the Rashba parameter with the crystal field Δ_{CF} induced by the polar displacements that alleviates the degeneracy of Ti t_{2g} states and annihilates the Rashba effects. Although α_R has intrinsically a linear dependance on polar displacements, the latter becomes antagonist to Rashba phenomena at large polar mode amplitude. Thus, the Rashba coefficient may be bound to an upper value.

DOI: 10.1103/PhysRevLett.132.106401

Spintronic exploits the spin degree of freedom in addition to the charge of carriers, yielding numerous applications in data storage [1]. Traditionally, spintronic relies on ferromagnetic metals such as Ni or Co as generators and detectors of spin currents. Nevertheless, ferromagnetic metals have several drawbacks: (i) they can generate undesired local magnetic fields hindering the densification of devices and (ii) a large voltage is required for reversing their magnetization, hence incompatible with our quest for low energy consumption devices. An alternative pathway toward lower power spintronics exists and exploits the spin-orbit interaction (SOI) of nonmagnetic materials through the spin Hall effect [2,3] and inverse spin Hall effect [4,5], alleviating the use of ferromagnets for generating spin currents [6].

More recently, a promising pathway toward efficient spin-charge current interconversion has been identified and uses a peculiar interplay between polar displacements and SOI: when inversion symmetry is broken, such as at interfaces or surfaces or in ferroelectric compounds, the polar displacements can yield a Rashba interaction that lifts the degeneracy of bands according to their spin [7]. For a polar axis along z, the Rashba SOI takes the following expression:

$$H_R = \alpha_R(S_y k_x - S_x k_y), \tag{1}$$

where α_R is the Rashba parameter ($\alpha_R \propto Q_P$, where Q_P is the polar displacement amplitude in the material), k_i is the momentum of electrons, and S_i is the spin direction ($i = x, y$). A spin locking is thus achieved with spins of carriers being orthogonal to the momentum k. Spin-to-charge current interconversions are then enabled through the Edelstein and inverse Edelstein effects [8,9], whose efficiency directly scales with the amplitude of the Rashba parameter [9].

At first glance, reaching a large Rashba phenomenon requires two key ingredients: (i) the material has to exhibit a sizable intrinsic SOI—i.e., large λ_{SO}—and (ii) the material must display large polar displacements amplitude. The latter criterion induces that α_R should scale linearly with the polar distortion amplitude while the former is usually reached for heavy elements and/or for compounds with highly degenerate states [10–12]. At interfaces or surfaces, polar displacements are pinned by the structure but ferroelectric materials offer a nonvolatile control of α_R through the reversal of polar displacements with an external electric field. However, structural displacements such as breathing distortions in $SrBiO_3$ associated with charge orderings [13] or octahedral rotations appearing in ferroelectric oxides [14] can tune the Rashba parameter. One may thus question whether "*the Rashba parameter always scales linearly with the polar displacements amplitude*" and whether "*the related structural displacements can tune α_R in a different manner*." It is important to clarify these questions as it could possibly unveil strategies to design compounds with larger Rashba parameters and possibly more efficient current interconversions.

In that context, strontium titanate perovskite oxide $SrTiO_3$ (STO) is a prototypical material for exploring the interplay between polar displacements and Rashba effects since (i) it enables efficient spin-to-charge current interconversion in the bidimensional electron gas (2-DEG) formed at its interface with $LaAlO_3$ [15]—albeit the

Rashba parameter is small, the efficiency of the interconversion also directly relies on the carrier lifetime that is large in STO—and (ii) oxide perovskites can be turned into ferroelectrics using various external stimuli [16]. In the bulk ground state, STO adopts a $I4/mcm$ tetragonal symmetry characterized by a $a^0a^0c^-$ O_6 group's rotations following Glazer's notations [17]—also called antiferrodistortive (AFD) motion—with respect to the perfectly undistorted $Pm\text{-}3m$ cubic cell existing at higher temperatures [Fig. 1(a)]. STO is a paraelectric at all temperatures but it becomes ferroelectric with a moderate epitaxial strain [18]. However, the strain phase diagram of STO is up to date rather elusive, hindering the identification of potentially interesting ferroelectric phases for spin-orbitronic applications.

In this Letter, I explore using *first-principles* simulations the phase diagram of $SrTiO_3$ experiencing compressive epitaxial strain and I reveal the existence of polar ground states for strain values η larger than 1.35% with respect to the bulk lattice parameter. The spontaneous polarization increases with increasing η until reaching a supertetragonal phase with a c/a ratio of 1.29 and a polarization approaching 100 $\mu C.cm^{-2}$. Within the ferroelectric phases, a Rashba spin splitting of the Ti t_{2g} bands located at the bottom of the conduction band is identified but the amplitude of the Rashba parameter is surprisingly found to diminish with the polar displacements' amplitude. This is due to the fact that polar displacements alleviate the Ti t_{2g} orbitals' degeneracies, thereby weakening the Rashba-SOI interaction. Ultimately, the phases with the largest polarizations do not show any Rashba spin splitting at the bottom of the conduction band. Thus, the interplay between polar displacements and the Rashba parameter is subtle in $SrTiO_3$ and preserving degenerate states rather than reaching high electrical dipoles might be a better route toward maximal Rashba parameters and more efficient spin-charge current interconversion.

Method.—First-principles density functional theory (DFT) calculations are performed with the Vienna *Ab initio* Simulation Package (VASP [19,20]) using the meta-Generalized Gradient Approximation (meta-GGA) Strongly Constrained and Appropriately Normalized (SCAN) exchange-correlation functional [21]. The SCAN functional was previously shown to be well suited for the study of perovskite oxides [22] and of ferroic properties of $ATiO_3$ compounds (A = Ba, Sr, Pb) [23], including the paraelectric nature of bulk STO (see Supplemental Material [17,24–31]). Epitaxial strain is modeled by imposing two lattice parameters to that of the substrate. Then, the third lattice parameter is allowed to relax in amplitude and direction and atomic positions are totally optimized until forces acting on each atom are lower than 0.001 eV/Å. In order to avoid getting trapped in false local minimums during geometry optimizations, several structures exhibiting (i) octahedral tilt patterns such as

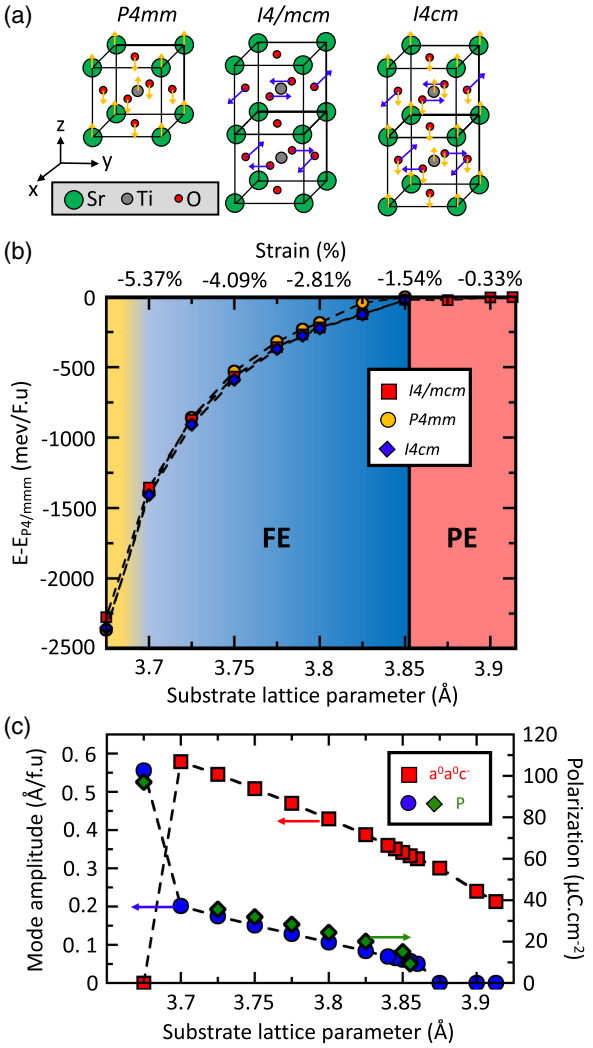

FIG. 1. Phase diagram of $SrTiO_3$ under compressive strain. (a) Sketches of the structural motions associated with the polar mode, the $a^0a^0c^-$ antiferrodistortive, and the combination of polar and antiferrodistortive motions yielding the $P4\,mm$, $I4/mcm$, and $I4cm$ cells, respectively. Arrows are not representative of the actual displacement amplitude appearing in the compound. (b) Energy difference (in meV/f.u) of most stable phases with respect to the high symmetry undistorted $P4/mmm$ cell of $SrTiO_3$ as a function of the strain. (c) Amplitudes (in Å/f.u) of polar (blue filled circles) and $a^0a^0c^-$ octahedral rotation distortions (red filled squares) extracted from a symmetry mode analysis with respect to the high symmetry undistorted $P4/mmm$ cell (left scale) and computed spontaneous polarization (in $\mu C.cm^{-2}$, green filled diamonds, right scale) for the identified ground states as a function of the strain.

$a^0a^0c^0$, $a^0a^0c^-$, $a^-a^0c^0$, $a^0a^0c^+$, $a^+a^0c^0$, $a^-a^-c^+$, $a^+a^-c^-$, or $a^-a^-c^-$ in Glazer's notation [17] as well as (ii) two polar axes either along or orthogonal to the substrate or no polar axis are considered as initial points for the structural relaxations. All relaxations are performed without the SOI, this interaction is only considered afterward for band structure calculations. The cutoff is set to

650 eV and is accompanied by a $8 \times 8 \times 6$ and $6 \times 6 \times 6$ kmesh for $(2\sqrt{2}, 2\sqrt{2}, 2)$ and (2,2,2) supercells of STO with respect the primitive high symmetry $Pm\text{-}3m$ cubic cell—four and eight formula units, respectively. Projector augmented wave potentials [32] are used with only treating d states as valence electrons for Ti cations. Wannier functions are built using the wannier90 package [33–37].

Strain phase diagram.—Figure 1(b) displays the total energy difference of the most stable structures relaxed with DFT with respect to the high symmetry $P4/mmm$ structure—the high symmetry primitive cell for epitaxially strained perovskites—as a function of the substrate lattice parameter. At low compressive strain ($|\eta| < 1.35\%$), STO adopts a centrosymmetric $I4/mcm$ cell very similar to the bulk material. This phase is characterized by a $a^0a^0c^-$ octahedral rotation pattern. Upon increasing the compressive strain between $1.35\% < |\eta| < 5.58\%$, a ferroelectric (FE) phase is identified adopting a $I4cm$ cell and displaying an additional polar axis along z with respect to the $I4/mcm$ cell [see sketches in Fig. 1(a)]. This result is reminiscent of the experimental observation of ferroelectricity in $SrTiO_3$ under a moderate compressive or tensile strain [18]. Finally, at a compressive strain of 6% ($a_{sub} = 3.675$ Å), STO adopts a FE $P4mm$ tetragonal structure [Fig. 1(a)] characterized by a polar axis along z and the total absence of any octahedral rotations. Surprisingly, a strong tetragonality with a c/a ratio of 1.29 is observed within this phase, while the structure stabilized at $a_{sub} = 3.69$ Å has a tetragonality of 1.19. This results hints at the "T-phase" stabilized for high compressive strain in $BiFeO_3$ [38,39] or in $BaTiO_3$ and $PbTiO_3$ under pressure [40–42]. It also relates with the ferroelectric phases predicted in perovskites undergoing high tensile strains [43,44]. These results suggest that a superferroelectric phase could be generic for perovskites experiencing large tensile and/or compressive strains.

Figure 1(c) reports the $a^0a^0c^-$ octahedral rotation and polar mode amplitudes extracted from a symmetry mode analysis with respect to a highly symmetric undistorted $P4/mmm$ cell as well as the computed spontaneous polarization as a function of the strain values. The spontaneous polarization—or polar mode amplitude—monotonously increases from 8.3 $\mu C.cm^{-2}$ ($|\eta| = 1.35\%$) to 41.7 $\mu C.cm^{-2}$ ($|\eta| = 5.58\%$) upon increasing the compressive strain value once the FE $I4cm$ phase is reached. Within the supertetragonal $P4mm$ phase, a giant polarization of 97 $\mu C.cm^{-2}$ is reached, again reminiscent of the situation reached in the T-phase of $BiFeO_3$ ($P = 150$ $\mu C.cm^{-2}$ [39]). The $a^0a^0c^-$ octahedral rotation amplitude also increases with increasing the strain value, suggesting that ferroelectricity and octahedral rotations are not strongly antagonists in strained $SrTiO_3$ [16,45]. This is consistent with Ref. [46], which previously showed that AFD motions and ferroelectricity can cooperate in $SrTiO_3$ once a sufficiently large tetragonality of the cell is achieved. These results are insensitive to the choice of the DFT exchange-correlation functional as the GGA Perdew Burke Ernzerhof revised for solid (PBEsol) DFT functional yields the very same trend with epitaxial strain (see Supplemental Material 2).

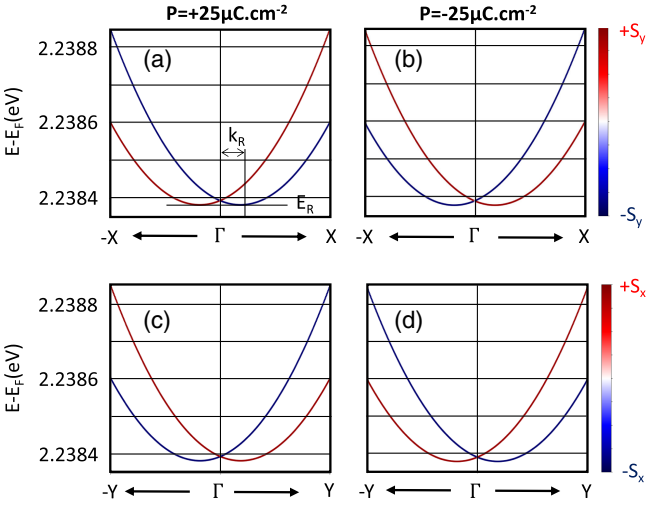

FIG. 2. Rashba spin splitting at the bottom of the conduction band in ferroelectric $SrTiO_3$. Bands dispersion along the Γ-X (a), (b) and Γ-Y (c),(d) paths projected on the S_x (c),(d) and S_y (a),(b) spin components for states at the bottom of the conduction band for a polarization up (a),(c) or down (b),(d). The ferroelectric state reached with a substrate lattice parameter of 3.80 Å is considered here. High symmetry points are $\Gamma(0,0,0)$, $X(½,0,0)$, and $Y(0,½,0)$ and refers to the $I4cm$ cell Brillouin zone.

Rashba parameters as a function of the polar mode amplitude.—Within the ferroelectric phases, STO lacks an inversion center since ions undergo polar displacements. This is similar to the situation appearing in 2-DEG formed in STO when a local symmetry breaking occurs at its surface and/or interface with other compounds. Hence, it can yield a Rashba spin-orbit effect with a spin splitting of the Ti-t_{2g} bands located at the bottom of the conduction band (CB) [15]. Figure 2(a) displays the band structure along the $\Gamma - X$ path associated with the bottom of CB for the $I4cm$ phase reached at 2.81% of compressive strain, this including the SOI. The degeneracy of bands at the bottom of CB is lifted according to the spin flavor $\pm S_y$, no $\pm S_x$ spin dependance is found for these bands—it is observed for bands dispersing along the $\Gamma - Y$ path [Fig. 2(c)]. Thus, a spin locking orthogonal to the momentum k of electrons and to the polar axis is identified, confirming the existence of Rashba phenomenon in polar STO. Finally, as observed in ferroelectric Rashba materials [13,14,47–50], a nonvolatile control of the spin locking is reached as switching the polarization reverses the band splitting [Figs. 2(b) and 2(d)].

Following the confirmation of the existence of Rashba states at the bottom of the conduction band of FE STO, the Rashba parameter α_R is extracted from DFT band structure calculations using the following formula $\alpha_R = (2E_R/k_R)$,

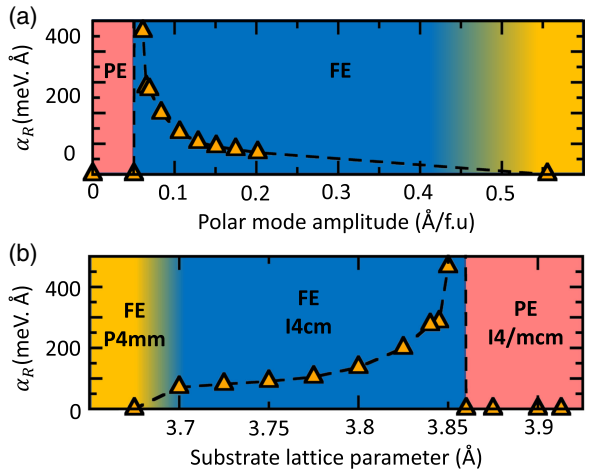

FIG. 3. Rashba parameter as a function of strain and polar displacements amplitude. Computed Rashba parameter α_R (in meV.Å) as a function of polar displacement amplitude [in Å/f.u, panel (a)] and substrate lattice parameter [in Å, panel (b)] in strained $SrTiO_3$ films.

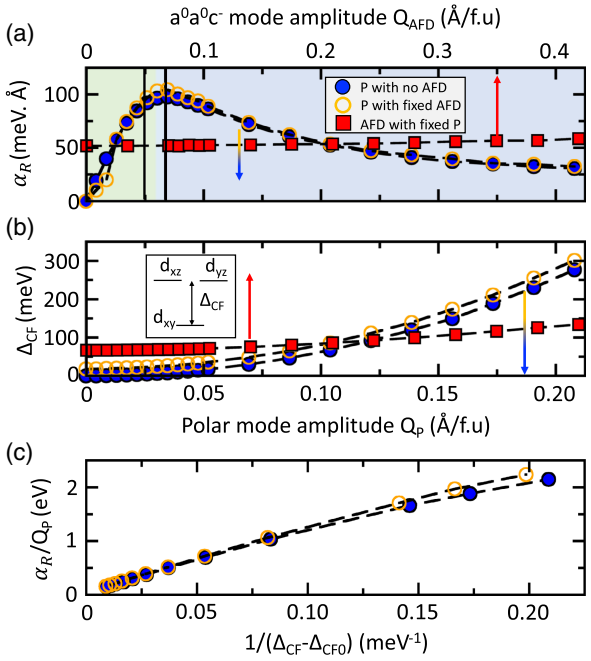

FIG. 4. Rashba parameter as a function of lattice distortions in a cubic $SrTiO_3$. (a),(b) Computed Rashba parameter [(a), in meV.Å, upper panel] and crystal field splitting Δ_{CF} [(b), meV, lower panel] between the d_{xy} and d_{xz}/d_{yz} orbitals as a function of the polar mode amplitude Q_P (in Å/f.u, lower scale) in a cubic cell of $SrTiO_3$ with (orange unfilled circles) and without (blue filled circles) $a^0a^0c^-$ AFD motions and as a function of AFD motion amplitude Q_{AFD} (in Å/f.u, upper scale, red filled squares) at a fixed polar amplitude. The amplitude of the frozen AFD motion is 0.296 Å/f.u (orange unfilled circles) and of the frozen polar mode amplitude is 0.104 Å/f.u (red filled squares). Only the states at the bottom of the conduction band are considered for extracting the Rashba parameter. (c) Normalized Rashba parameter α_R/Q_P (meV) as a function of the inverse of the crystal field splitting induced by the polar displacement. Δ_{CF0} is the crystal field splitting appearing at $Q_P = 0$ Å.

where E_R is the energy splitting with respect to the high symmetry positions and k_R is the momentum offset [see Fig. 2(a)]. Figures 3(a) and 3(b) summarize the evolution of α_R as a function of the polar mode and strain amplitudes, respectively. The Rashba coefficient α_R is estimated between 10 to 100 meV.Å, an order of magnitude in agreement with the 30 meV.Å estimated experimentally for the 2-DEG appearing at the $LaAlO_3/SrTiO_3$ interface. Nevertheless, α_R monotonously decreases with the polar mode amplitude and even reaches 0 within the super-tetragonal phase despite the latter phase shows the largest spontaneous polarization ($P = 97$ μC.cm^{-2}). By looking at the evolution of α_R with the substrate lattice parameter [Fig. 3(b)], α_R in fact diverges and reaches a maximal value at the boundary between the ferroelectric-paraelectric phases reached under epitaxial strain. Such a behavior is surprising since the Rashba coefficient should *a priori* scale linearly with the polar displacement amplitude.

The Rashba parameter is dominated by polar displacement amplitude in two different regimes.—In order to understand the surprising behavior of α_R as a function of epitaxial strain or polar mode amplitude, it is important to disentangle the contribution of the distortions appearing in the materials on α_R, namely octahedral rotations and polar displacements. To that end, the calculation of α_R is performed within a perfectly undistorted cubic cell of $SrTiO_3$ as a function of the polar and AFD mode amplitude Q_P and Q_{AFD}, respectively. Results are summarized in Fig. 4(a). Starting from the cubic cell with only the polar mode condensed, α_R first exhibits a linear trend as a function of Q_P for $Q_P < 0.025$ Å/f.u and then it becomes inversely proportional to Q_P (i.e., $\alpha_R \propto (1/Q_P)$) for $Q_P > 0.025$ Å/f.u. Adding a fixed octahedral rotation within the cubic cell with an amplitude $Q_{AFD} = 0.210$ Å/f.u, the trend and values of α_R as a function of Q_P are not substantially modified. The minor role of octahedral rotations is confirmed by performing the calculation of α_R as a function of Q_{AFD} at fixed polar displacement amplitude $Q_P = 0.104$ Å/f.u that shows a nearly constant α_R—it only increases by 12% between $Q_{AFD} = 0$ Å/f.u and $Q_{AFD} = 0.420$ Å/f.u. Therefore, one concludes here that polar displacements are the key factor behind the trend of α_R versus the epitaxial strain.

The polar displacements alleviate t_{2g} states degeneracies and annihilate the Rashba phenomena.—The next step is to understand the two Q_P ranges producing either a proportional or inversely proportional trend between α_R and Q_P. In a perfectly undistorted cell of $SrTiO_3$, the three t_{2g} states are perfectly degenerate. However, the lattice distortions can introduce a crystal field splitting Δ_{CF}

alleviating the degeneracy of the t_{2g} states. Figure 4(b) displays the evolution of $\Delta_{CF} = E_{dxz/dyz} - E_{dxy}$ as a function of the different lattice mode amplitude where $E_{dxy,dxz,dyz}$ are the on-site energies of the t_{2g} orbitals obtained by a construction of atomiclike Wannier functions centered on Ti cations—only the Kohn-Sham states associated with t_{2g} states are considered for the construction, i.e., 12 states for a 4 f.u of STO. Firstly, polar displacements produce a strong Δ_{CF} with $\Delta_{CF} = 6314Q_P^2$, whose evolution is not altered by the introduction of AFD motions—only the crystal field at zero mode amplitude Δ_{CF0} is shifted to higher values by the introduction of AFD motion—while octahedral rotation brings a contribution to Δ_{CF} that is 1 order of magnitude smaller with $\Delta_{CF} - \Delta_{CF0} = 395Q_{AFD}^2$. Secondly, similarly to α_R, one recovers two distinct regimes for Δ_{CF} as a function of Q_P: (i) Δ_{CF} is constant for $Q_P < 0.025$ Å/f.u, while (ii) it becomes sizable and large for $Q_P > 0.025$ Å/f.u. Possessing two regimes as a function of Q_P, Δ_{CF} and α_R may be connected together.

α_R is inversely proportional to Δ_{CF}.—Figure 4(c) displays the evolution of (α_R/Q_P) as a function of $1/(\Delta_{CF} - \Delta_{CF0})$ for the $Q_P > 0.0025$ Å/f.u regime. A clear linear trend between the inverse crystal field splitting induced by polar displacements and the normalized Rashba parameter is identified, either in the presence or not of octahedral rotation. Thus, although α_R is proportional to Q_P by construction of the SOI, it is inversely proportional to the crystal field splitting of states undergoing the Rashba phenomena. The latter observation is compatible with the results of Bahramy *et al.*, who showed that the amplitude of α_R scales as $1/(E_m\text{-}E_n)$ where $E_m\text{-}E_n$ are the energies of states m and n experiencing the Rashba effects [10]. Nevertheless, the observed effect in $SrTiO_3$ is subtle: (i) in all situations, α_R scales as (Q_P/Δ_{CF}) but (ii) at small polar displacement (i.e., $Q_P < 0.025$ Å/f.u), α_R scales linearly with Q_P since Δ_{CF} is almost constant and (iii) for $Q_P > 0.025$ Å/f.u, the $(1/\Delta_{CF}) \propto (1/Q_P^2)$ contribution to α_R dominates and hence α_R ultimately evolves as $(1/Q_P)$. This is compatible with the trend of α_R as a function of Q_P of Fig. 4(a). It further explains the surprising trend of α_R with epitaxial strain of Fig 3(b). At low compressive strain, the polar displacements are small and Δ_{CF} is close to zero, hence producing large α_R and even diverging at the paraelectric-ferroelectric boundary. At larger compressive strain, including the supertetragonal phase, polar displacements alleviate t_{2g} states degeneracies and hence annihilate the Rashba SOI. Finally, it is worth emphasizing that the computed α_R in compressively strained compounds is larger than the one computed in a perfect cubic cell at fixed polar mode amplitude. This is due to an additional crystal field splitting of Ti t_{2g} orbitals induced by the compressive strain that promotes the stabilization of the d_{xz}/d_{yz} orbitals over the d_{xy} orbital, in opposition to the polar mode, hence diminishing the overall crystal field acting on Ti t_{2g} states.

Conclusion.—Although α_R is often expected to monotonously scale with the polar mode amplitude by construction of the SOI, the polar displacements can alleviate the degeneracy of the Ti t_{2g} states and quench the Rashba SOI. Consequently, the Rashba parameter is bound to an upper value. Preserving the Ti t_{2g} orbital degeneracies over searching for larger electrical dipoles is thus the key to achieve large Rashba parameters in STO. Although applied in this Letter to ferroelectric phases of STO reached under compressive epitaxial strain, the concept is in fact general to any material showing polar displacements of atoms undergoing the Rashba SOI. For instance, one may consider playing with epitaxial strain in order to modify the Ti t_{2g} states degeneracies appearing in the 2-DEG for reaching more efficient spin-to-charge current interconversions [15].

J. V. acknowledged discussion with M. Bibes, L. Vila, and J. P. Attané. J. V. acknowledges access granted to High Performance Computing resources of Criann through the projects 2020005 and 2007013 and of Cines through the DARI project A0080911453. This work was supported by the French ANR through the project "CONTRABASS".

[1] C. Chappert, A. Fert, and F. N. Van Dau, Nat. Mater. **6**, 813 (2007).
[2] M. I. D'yakonov and V. I. Perel', Sov. J. Exp. Theor. Phys. Lett. **13**, 467 (1971).
[3] Y. K. Kato, R. C. Myers, A. C. Gossard, and D. D. Awschalom, Science **306**, 1910 (2004).
[4] K. Ando and E. Saitoh, Nat. Commun. **3**, 629 (2012).
[5] H. Zhao, E. J. Loren, H. M. van Driel, and A. L. Smirl, Phys. Rev. Lett. **96**, 246601 (2006).
[6] L. Liu, C. F. Pai, Y. Li, H. W. Tseng, D. C. Ralph, and R. A. Buhrman, Science **336**, 555 (2012).
[7] Y. A. Bychkov and E. I. Rashba, JETP Lett. **39**, 78 (1984).
[8] V. M. Edelstein, Solid State Commun. **73**, 233 (1990).
[9] J. C. R. Sánchez, L. Vila, G. Desfonds, S. Gambarelli, J. P. Attané, J. M. De Teresa, C. Magén, and A. Fert, Nat. Commun. **4**, 2944 (2013).
[10] M. S. Bahramy, R. Arita, and N. Nagaosa, Phys. Rev. B **84**, 041202(R) (2011).
[11] A. Joshua, S. Pecker, J. Ruhman, E. Altman, and S. Ilani, Nat. Commun. **3**, 1129 (2012).
[12] K. V. Shanavas, Z. S. Popović, and S. Satpathy, Phys. Rev. B **90**, 165108 (2014).
[13] J. Varignon, J. Santamaria, and M. Bibes, Phys. Rev. Lett. **122**, 116401 (2019).
[14] H. Djani, A. C. Garcia-Castro, W. Y. Tong, P. Barone, E. Bousquet, S. Picozzi, and P. Ghosez, npj Quantum Mater. **4**, 51 (2019).
[15] E. Lesne, Y. Fu, S. Oyarzun, J. C. Rojas-Sánchez, D. C. Vaz, H. Naganuma, G. Sicoli, J.-P. Attané, M. Jamet, E. Jacquet,

J.-M. George, A. Barthélémy, H. Jaffrès, A. Fert, M. Bibes, and L. Vila, Nat. Mater. **15**, 1261 (2016).
[16] J. Varignon, N. C. Bristowe, É. Bousquet, and P. Ghosez, Phys. Sci. Rev. **5**, 0069 (2019).
[17] A. M. Glazer, Acta Crystallogr. Sect. B **28**, 3384 (1972).
[18] J. H. Haeni, P. Irvin, W. Chang, R. Uecker, P. Reiche, Y. L. Li, S. Choudhury, W. Tian, M. E. Hawley, B. Craigo, A. K. Tagantsev, X. Q. Pan, S. K. Streiffer, L. Q. Chen, S. W. Kirchoefer, J. Levy, and D. G. Schlom, Nature (London) **430**, 758 (2004).
[19] G. Kresse and J. Haffner, Phys. Rev. B **47**, 558 (1993).
[20] G. Kresse and J. Furthmüller, J. Comput. Mater. Sci. **6**, 15 (1996).
[21] J. Sun, A. Ruzsinszky, and J. P. Perdew, Phys. Rev. Lett. **115**, 036402 (2015).
[22] J. Varignon, M. Bibes, and A. Zunger, Phys. Rev. B **100**, 035119 (2019).
[23] Y. Zhang, J. Sun, J. P. Perdew, and X. Wu, Phys. Rev. B **96**, 035143 (2017).
[24] See Supplemental Material at http://link.aps.org/supplemental/10.1103/PhysRevLett.132.106401 for technical details and additional results supporting the findings described in the Letter, which includes Refs. [25–31].
[25] K. A. Müller, W. Berlinger, and F. Waldner, Phys. Rev. Lett. **21**, 814 (1968).
[26] S. Pal, N. Strkalj, C. J. Yang, M. C. Weber, M. Trassin, M. Woerner, and M. Fiebig, Phys. Rev. X **11**, 021023 (2021).
[27] Y. Zhang, J. Sun, J. P. Perdew, and X. Wu, Phys. Rev. B **96**, 035143 (2017).
[28] D. Shin, S. Latini, C. Schäfer, S. A. Sato, U. De Giovannini, H. Hübener, and A. Rubio, Phys. Rev. B **104**, L060103 (2021).
[29] M. Takesada, M. Itoh, and T. Yagi, Phys. Rev. Lett. **96**, 227602 (2006).
[30] *Ferroelectrics, and Related Substances: Oxides, Landolt-Bornstein*, New Series Group III Vol. 3, edited by K. H. Hellwege and A. M. Hellwege (Springer-Verlag, Berlin, 1969).
[31] K. Tsuda and M. Tanaka, Acta Crystallogr. Sect. A **51**, 7 (1995).
[32] P. E. Blöchl, Phys. Rev. B **50**, 17953 (1994).
[33] G. Pizzi *et al.*, J. Phys. Condens. Matter **32**, 165902 (2020).
[34] I. Souza, N. Marzari, and D. Vanderbilt, Phys. Rev. B **65**, 035109 (2001).
[35] N. Marzari and D. Vanderbilt, Phys. Rev. B **56**, 12847 (1997).
[36] A. A. Mostofi, J. R. Yates, G. Pizzi, Y. S. Lee, I. Souza, D. Vanderbilt, and N. Marzari, Comput. Phys. Commun. **185**, 2309 (2014).
[37] A. A. Mostofi, J. R. Yates, Y.-S. Lee, I. Souza, D. Vanderbilt, and N. Marzari, Comput. Phys. Commun. **178**, 685 (2008).
[38] A. J. Hatt, N. A. Spaldin, and C. Ederer, Phys. Rev. B **81**, 054109 (2010).
[39] D. Sando, A. Barthélémy, and M. Bibes, J. Phys. Condens. Matter **26**, 473201 (2014).
[40] S. Mellaerts, J. W. Seo, V. Afanas'ev, M. Houssa, and J.-P. Locquet, Phys. Rev. Mater. **6**, 064410 (2022).
[41] J. Sun, Q. Li, H. Zhu, Z. Liu, K. Lin, N. Wang, Q. Zhang, L. Gu, J. Deng, J. Chen, and X. Xing, Adv. Mater. **32**, 2002968 (2020).
[42] J. Wang, B. Wylie-Van Eerd, T. Sluka, C. Sandu, M. Cantoni, X. K. Wei, A. Kvasov, L. J. McGilly, P. Gemeiner, B. Dkhil, A. Tagantsev, J. Trodahl, and N. Setter, Nat. Mater. **14**, 985 (2015).
[43] Y. Yang, W. Ren, M. Stengel, X. H. Yan, and L. Bellaiche, Phys. Rev. Lett. **109**, 057602 (2012).
[44] J. Varignon, N. C. Bristowe, and P. Ghosez, Phys. Rev. Lett. **116**, 057602 (2016).
[45] N. A. Benedek and C. J. Fennie, J. Phys. Chem. C **117**, 13339 (2013).
[46] U. Aschauer and N. A. Spaldin, J. Phys. Condens. Matter **26**, 122203 (2014).
[47] S. Picozzi, Front. Phys. **2**, 10 (2014).
[48] M. Liebmann, C. Rinaldi, D. Di Sante, J. Kellner, C. Pauly, R. N. Wang, J. E. Boschker, A. Giussani, S. Bertoli, M. Cantoni, L. Baldrati, M. Asa, I. Vobornik, G. Panaccione, D. Marchenko, J. Sánchez-Barriga, O. Rader, R. Calarco, S. Picozzi, R. Bertacco, and M. Morgenstern, Adv. Mater. **28**, 560 (2016).
[49] D. Di Sante, P. Barone, R. Bertacco, and S. Picozzi, Adv. Mater. **25**, 509 (2013).
[50] L. G. D. Da Silveira, P. Barone, and S. Picozzi, Phys. Rev. B **93**, 245159 (2016).